The Clay Minerals Society Workshop Lectures Series, Vol. 21 (2016), Chapter 5, 53–64

HIGH-SPEED, COUPLED MICRO-BEAM XRD/XRF/XAFS MAPPING AT GSECARS: APS BEAMLINE 13-ID-E

Antonio Lanzirotti[1]*, Matt Newville[1], Lori Manoukian[2], and Karina Lange[3]

[1]*Center for Advanced Radiation Sources, The University of Chicago, Chicago, IL 60637, USA*
[2]*Department of Geological Sciences and Engineering, Queen's University, Kingston, ON, Canada*
[3]*Canadian Nuclear Safety Commission, Ottawa, ON, Canada*
**e-mail: lanzirotti@uchicago.edu*

The present study describes new instrumentation developments at the GSECARS 13-ID-E hard X-ray microprobe beamline at the Advanced Photon Source that allows for high-speed, coupled micro-beam X-ray diffractions/X-ray fluorescence/X-ray absorption fine structure mapping. These new methodologies provide Earth and environmental scientists with unique coupled tools for evaluating microscale mineralogical and chemical heterogeneities in fine-grained sediments, soils, shales, and mine tailings and associated secondary precipitates. In particular, new technologies and approaches for integrating fast μXRD mapping into routine X-ray microprobe beamline operations are described and several real-world examples are given of how this approach provides unique insights with regards to micrometer-scale heterogeneities in mineralogy and chemistry that are difficult to obtain by other methods. Examples described here include waste streams associated with mine tailings from the McClean Lake mining facility located on the eastern edge of the Athabasca Basin in northern Saskatchewan, Canada, and from mine-drainage waters from the epithermal Au-Ag-Cu deposits of the Lagunas Norte mine in the Peruvian Andes.

1. Introduction

Synchrotron hard X-ray scanning probe beamlines that traditionally have focused on the scientific applications of micro- and nano-focused X-ray fluorescence microscopy (μXRF) and absorption fine structure spectroscopies (μXAFS) now rather routinely incorporate large two-dimensional area detectors that provide researchers with micro-focused X-ray diffraction (μXRD) capabilities as well. Researchers can now couple spatially resolved information about the chemical state of a material to data which identify the crystalline phases present in a sample, phase structure, and mineral orientation or strain at the micrometer scale. For Earth and environmental scientists in particular, being able to interrogate materials that exhibit high degrees of heterogeneity in chemistry and mineralogy using coupled μXRF, μXAFS, and μXRD can provide clarity about fine-scale mineralogical and chemical changes that may occur within and

DOI: 10.1346/CMS-WLS-21.5

between components in soils, rocks, and environmental wastes, within fractures in geologic materials, or aid in identifying biogenic mineral precipitates within organisms, among other benefits (Tamura *et al.*, 2002; Treiman *et al.*, 2004; Jackson *et al.*, 2005; Walker *et al.*, 2005; Lange *et al.*, 2010).

Modern X-ray fluorescence microscopy (XFM) beamlines also now routinely utilize a new generation of advanced energy dispersive fluorescence detectors and digital signal processors with high data acquisition rates that allow for rapid, continuous scanning of samples with typical pixel dwell times in the millisecond and sub-millisecond range. These systems have been scientifically transformative in enabling XFM beamlines to provide megapixel imaging of X-ray fluorescence at micrometer scales (Vogt and Lanzirotti, 2013). Unfortunately, to date, it has not been feasible generally to provide μXRD data in this modality as the most commonly used CCD-based area detectors typically require acquisition times of >1 s and the use of an integrated photon shutter that allows for detector readout between frames without incident X-rays on the detector sensor. While these CCD-based detectors generally provide excellent pixel resolution and dynamic range, the relatively slow readout rates make them impractical for use in continuous, fast-scanning μXRD mapping that can be coupled to fast μXRF imaging.

A new generation of digital flat-panel detectors, optimized for XRD, which provides capabilities for high data throughput and real-time imaging of diffracted X-rays from a sample, is now available. These detectors can be incorporated into an XFM beamline configuration to enable high-speed, coupled μXRD/μXRF/μXAFS mapping. For continuous μXRD mapping, these detectors are advantageous in that they do not require use of a photon shutter and can collect data at high frame rates. Such detectors can collect data at rates faster than 30 frames per second (fps) while maintaining high resolution, good dynamic range, and contrast. This translates to an acquisition time of 30 milliseconds (ms) per pixel or faster if data are collected in an imaging modality synchronous with μXRF data collection, a reasonably fast scan rate for megapixel imaging of XRD in a heterogeneous material.

The present article describes the implementation and utilization of these detectors at the GSECARS 13-ID-E hard X-ray microprobe beamline at the Advanced Photon Source (APS) for high-speed, coupled μXRD/μXRF/μXAFS mapping. Examples are presented that illustrate the potential application of these new methodologies for evaluating microscale mineralogical and chemical heterogeneities in fine-grained sediments and mine tailings. Here, the application of this methodology to the evaluation of the chemistry and mineralogy of waste streams associated with mine tailings from the McClean Lake mining facility located on the eastern edge of the Athabasca Basin in northern Saskatchewan, Canada, and from mine-drainage waters from the epithermal Au-Ag-Cu deposits of the Lagunas Norte mine in the Peruvian Andes are described.

2. Materials and methods

Data were collected at the 13-ID-E beamline at the APS, Argonne National Laboratory, Chicago, Illinois, USA (Figure 1). Beamline 13-ID-E is an undulator-based (3.6 cm

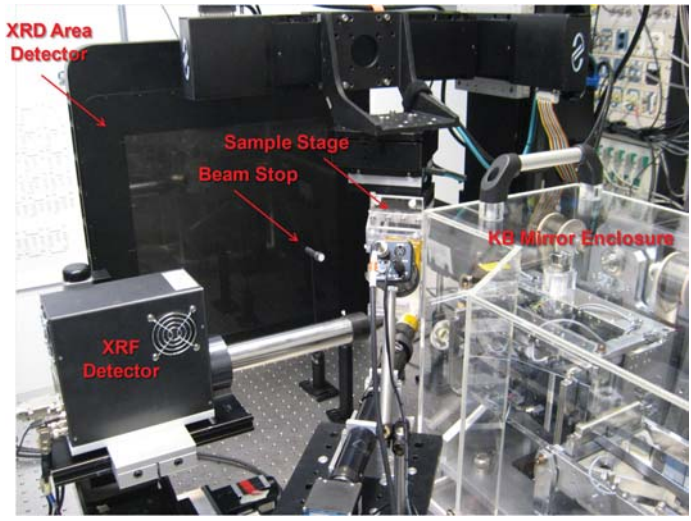

Figure 1. Photograph of the beamline 13-ID-E experimental station configured for coupled μXRD/μXRF/μXAFS mapping. The μXRD area data is collected using a Perkin-Elmer 16-inch amorphous silicon digital X-ray detector (XRD1621), shown in a transmission-mode geometry downstream from the sample. Coupled to the 13-ID-E microprobe, such devices provide the ability to perform near real-time μXRD for characterization, imaging, and tomography synchronous with μXRF mapping.

period U36 undulator in a canted geometry), hard X-ray microprobe instrument which utilizes dynamically figured, grazing incidence silicon mirrors placed in a Kirkpatrick-Baez geometry for X-ray focusing. The 13-ID-E optics provide a focused spot size to the sample of $\sim 1 \times 2$ μm (H × V) with a photon flux of $\sim 10^{11}$ photons/s within this focused spot. The 13-ID-E monochromator is a liquid nitrogen cryo-cooled, air-bearing, double-crystal monochromator (Instrument Design Technology Ltd., Cheshire, UK) which sits 25 m from the U36 source; it provides monochromatic X-rays with a spectral range from 2.4 to 28 keV ($\Delta E/E \approx 1.1 \times 10^{-4}$) suitable for both microfocused XANES and EXAFS. Two horizontally deflecting silicon mirrors downstream from the monochromator focus the beam to create a secondary horizontal source at a set of high-stability, precision slits 40 m from the U36 source. This secondary source is then re-imaged in the experimental station.

X-ray fluorescence from samples is measured using a 4-element Vortex ME4 (Hitachi Inc.) silicon drift diode detector sitting at 90° to the incident beam and in the plane of the storage ring. The ME4 is coupled to an Xspress 3 digital X-ray multi-channel analyzer system (Quantum Detectors). The Xspress 3 digital spectrometer can put out count rates of up to ~3 Mcps from the ME4 detector. To measure XRD from the sample, a Perkin Elmer XRD1621 digital flat panel detector placed in transmission geometry ~400 mm downstream from the sample was used. The XRD1621 detector uses a 41 cm × 41 cm amorphous silicon sensor with a 2048 × 2048 sensor size. The XRD1621 provides 200 μm pixel resolutions at 1 × 1 binning, frame rates of 15 fps at 1 × 1 binning,

and 30 fps at 2 × 2 binning. In the coupled μXRF/μXRD mapping mode, both the XRF and XRD detectors are triggered by trigger pulses generated by a Newport XPS motor controller which is used to control sample-stage motion. An XPS controller trigger pulse generated for each pixel is routed to the channel advance input of a Struck SIS3820 multichannel scaler which in turn is routed to the trigger inputs of the Xspress 3 and XRD1621 systems. For the studies presented here, the area detector positioning covers a Q range up to ~5 $Å^{-1}$.

The μXAFS point spectra presented were collected at the As K-edge (Figure 2 right). Arsenic oxidation state maps (Figure 2 lower left) were generated by imaging the AsKα

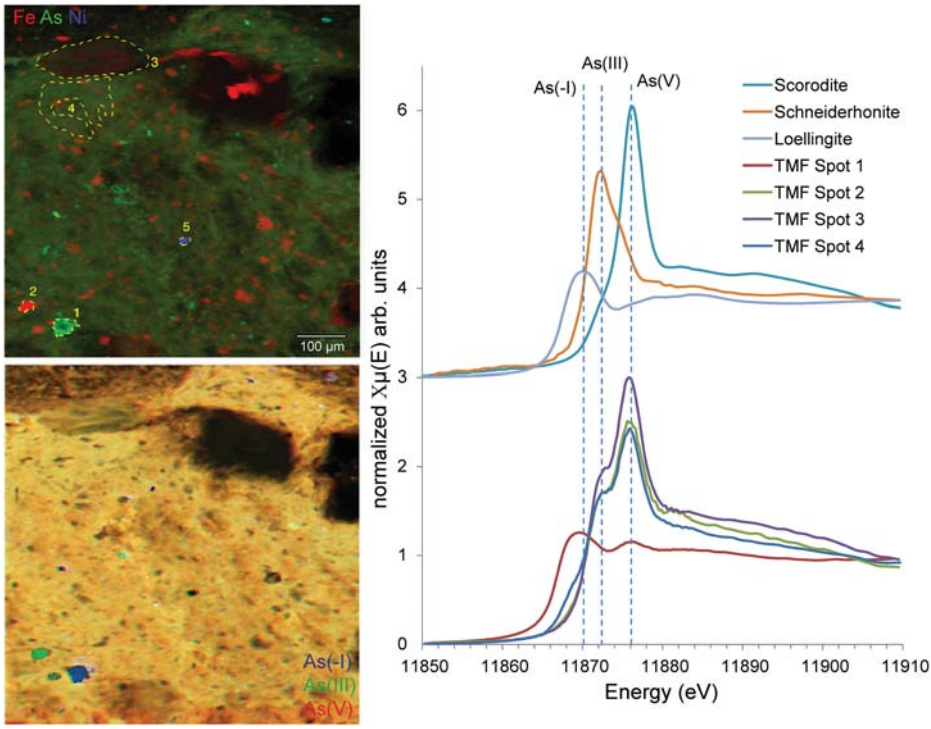

Figure 2. (Top left) A three-color, RGB compositional map of the intensity of Fe (red), As (green), and NiKα (blue) fluorescence in a thin section of mine-tailings material from the McClean Lake tailings management facility. The maximum intensity of each emission line is scaled arbitrarily for easier visualization. The image is 600 μm across, each pixel represents acquisition of full XRF energy dispersive spectra every 2 μm at a rate of 100 ms. The yellowed dashed areas labeled 1 through 5 show areas where XRD area detector data shown in Figure 3 were summed for analysis. (Bottom left) An RGB map showing the relative distribution of varying oxidation states of arsenic in the same map. As(-I) is shown in blue, As(III) in green, and As(V) in red. (Right) Plotted are spot μXAFS spectra of arsenic for a point roughly within the center of summed areas 1–4 shown in the upper left figure. Also, for reference, XAFS spectra for As(-I) loellingite, As(III) schneiderhonite, and As(V) reference materials are shown. Comparison of XAFS spectra show that most of the McClean Lake sample analyzed here is dominated by As(V) but with varying amounts of As(III) also present. Some As(-I) phases also can be found.

emission intensity measured at incident beam energies corresponding to the white line maxima for As(-I), As(III), and As(V) (as measured in loellingite, schneiderhonite, and scorodite standards) and then normalized to an intensity measured on the edge step (11905 eV). The μXRF and μXRD compositional maps presented here were collected using an incident beam energy of 17.5 keV. A two-dimensional, continuous mapping mode was used to collect these coupled μXRF/μXRD maps with the sample stage scanned continuously and bi-directionally through the focused, incident beam. Mapping data presented here were collected at frame rates between 50 and 100 ms per pixel. Calibration and integration of powder XRD data were done using the *Dioptas* program (Prescher, 2014) developed at GSECARS, which is freely available for interested users (https://github.com/Dioptas/Dioptas).

For the demonstration studies discussed here, coupled μXRF/μXRD/μXAFS data were collected from mine-waste samples that have been resin embedded and prepared as thin sections. All analyses were conducted under ambient conditions. The first example is from a sample of mine tailings from the McClean Lake Tailings Management Facility (TMF). McClean Lake is a uranium mining and processing facility located on the eastern edge of the Athabasca Basin in northern Saskatchewan, Canada. Contaminant release from the TMF is, in part, controlled geochemically and designed to maintain the concentrations of contaminants such as As and Ni at low levels in the tailings porewater. The thin section analyzed was prepared from a tailings core sample that was resin embedded, sectioned to 30 μm thickness, and mounted to a pure quartz glass substrate. The μXRD data, collected in transmission mode geometry, are acquired through the glass substrate for this sample.

The second dataset described here measures secondary precipitates collected from mine drainage waters seeping from the pit wall of the Lagunas Norte mine in Peru. The Lagunas Norte ore deposit is a Miocene, high-sulfidation, epithermal Au-Ag-Cu deposit (Montgomery, 2012) located 140 km east of the city of Trujillo in the Peruvian Andes. After collection, these precipitates were impregnated with epoxy (Epo-tek 301) and made into doubly polished 35 μm thin sections. These sections are designed to be lifted from their glass substrate for XFM analysis.

3. Results and discussion

3.1. McClean lake tailings management facility, Saskatchewan, Canada

One of the primary controls for managing waste streams at the McClean Lake TMF is geochemical, achieved through careful addition of ferric iron to waste material and pH adjustment after uranium extraction. This geochemical control is designed to, over time, convert ore arsenides (primarily niccolite) to stable arsenates (such as scorodite) which are disposed of within the tailings disposal site (Mahoney *et al.*, 2007). Synchrotron μXRF/μXRD/μXAFS mapping of these samples shows that these materials are a complex and heterogeneous mixture of mineral phases variably enriched in Fe, As, and Ni, representing original ore minerals that have survived milling and processing, residual iron oxides from the ore, and new iron- and arsenic-bearing precipitates that

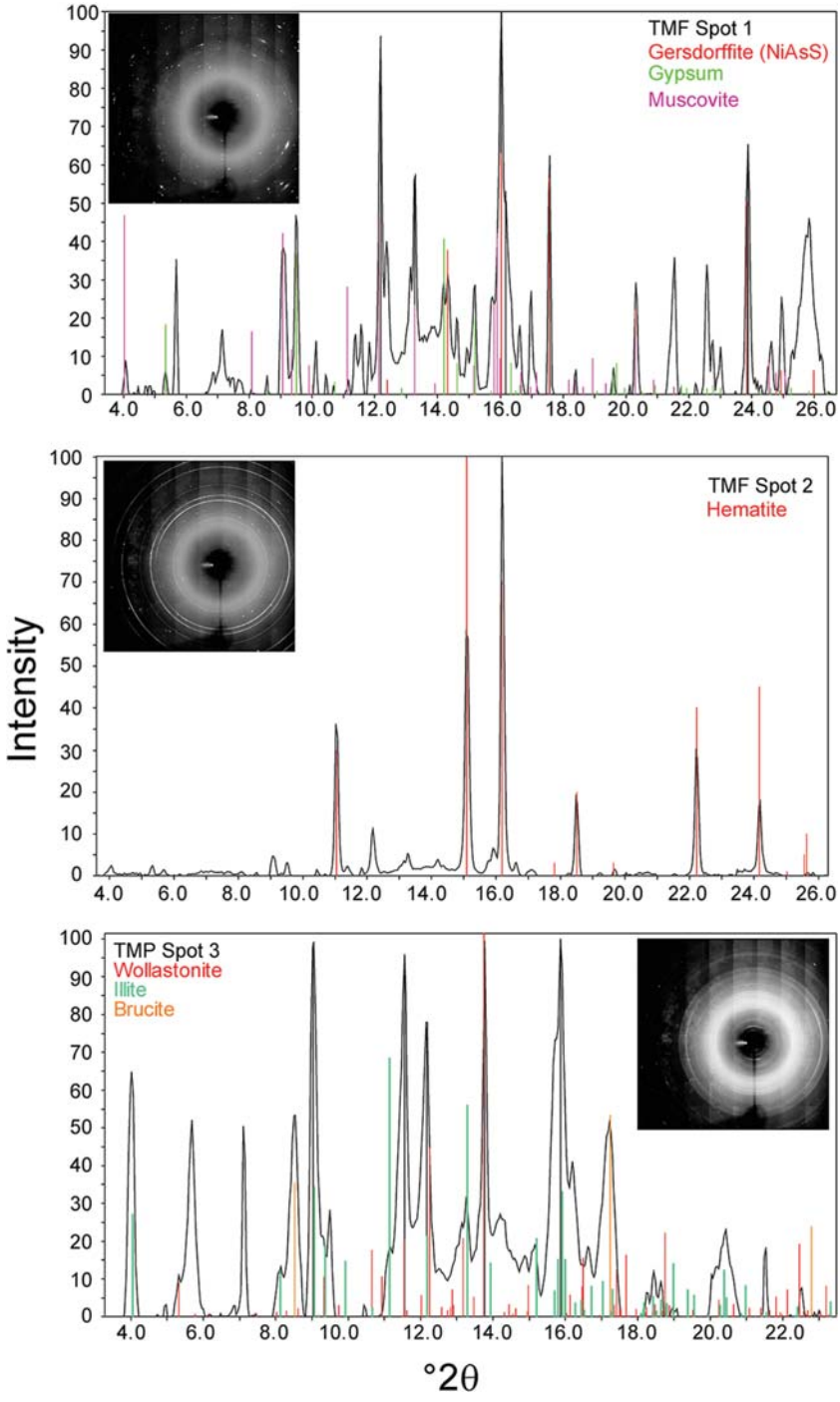
TMF Spot 1
Gersdorffite (NiAsS)
Gypsum
Muscovite
TMF Spot 2
Hematite
TMP Spot 3
Wollastonite
Illite
Brucite
Intensity
°2θ

have formed in response to addition of ferric iron after ore extraction. Identifying these components uniquely at the microscale to evaluate the progression of geochemical conversion of arsenic waste to oxidized species with time is challenging. Ideally, at the microscale, it would be most useful to identify the mineral phases to which each molecular species is bound or sorbed.

A 300 × 300 pixel (600 μm × 600 μm) μXRF compositional map for Fe, As, and NiKα fluorescence (upper left) and a comparable oxidation state map (lower left) of the distribution of As(-I), As(III), and As(V) species in a sample of this material is shown in Figure 2. These maps were collected in continuous scanning mode with a 2 μm pixel size at a scan rate of 100 ms/pixel. Both maps clearly show microscale heterogeneity in terms of both the abundance of these elements and the oxidation state of arsenic. The latter is also illustrated by more detailed point μXAFS analyses (Figure 2, right) and both point μXAFS and mapping show that while arsenic is mostly present in the As(V) oxidation state, both As(III) and As(-I) species can also be found. From the μXRF and μXAFS data alone, however, we cannot distinguish uniquely within which mineral phases these molecular species are incorporated or to which mineral phases they are bound.

The ability of μXRD mapping to image the spatial distribution of mineral phases directly provides researchers with a high-sensitivity and high-resolution method for evaluating in these samples the reaction progress over time as a function of mineralogy, chemical composition, and molecular speciation. Because every map pixel contains an independent XRD frame (90,000 of them), regions of interest can, therefore, be defined on the map based on unique chemical features, *e.g.* areas of elevated nickel abundance or areas where arsenic is found as a reduced species. The XRD frames within each Region of Interest (ROI) are then summed to provide an averaged XRD pattern for that area and taking advantage of the pixel averaging that summation provides to improve statistics and produce more powder-like patterns (Figure 3). Such data can provide unequivocal mineralogical identification, particularly when coupled with elemental information, and allows for unique characterization of how chemical species are bound to specific mineral phases. In the data shown in Figures 2 and 3, for example, areas can be delineated (TMF spot 1) which are elevated in both Ni and As abundance (*via* μXRF), contain As(-I) as a reduced arsenic species (*via* μXAFS), and show the presence of NiAsS in the mineralogy (*via* μXRD). All observations are consistent with the presence of original nickel arsenide ore minerals. In the same map areas (TMF spot 2), spots can also be identified which are high in

Figure 3. As every pixel in the McClean Lake map shown in Figure 2 contains an independent μXRD area detector frame, summation of frames in the regions shown in Figure 2 provides more powder-like patterns. Shown are both the summed area detector frame generated as an inset and the integrated °2θ *vs.* intensity patterns for three of these areas: ROI1 (296 pixels), ROI2 (141 pixels), and ROI3 (2322 pixels) with identified mineralogy based on the XRD patterns (shown as colored overlays of standard reflections and intensities). The mineralogy that is identified is consistent with both the chemical composition measured using μXRF and with arsenic oxidation state measured using μXAFS.

Fe (μXRF) where hematite is the dominant mineral phase (μXRD) and As is in the oxidized As(V) state (μXAFS), probably reflecting arsenates sorbed to ferric iron added post ore extraction.

3.2. Lagunas Norte Au-Ag-Cu Mine, Peru

The long-term objective of studying secondary precipitates in waste waters from the Lagunas Norte mine is to investigate methods of extracting metals from acid mine waste in order to minimize the environmental impact of the drainage and to offset remediation costs. Bulk XRD analysis of the secondary precipitates collected (Philips X-Pert, Queen's University, Kingston, Ontario, Canada) shows that these materials are sulfate-dominated, including mineral phases such as chalcanthite ($CuSO_4 \cdot 5H_2O$) and gypsum ($CaSO_4 \cdot 2H_2O$). Given the wide range of metals that are associated with these deposits (Au, Fe, Al, Cu, As, Zn, Cd, Te, Hg), understanding their relationship to the secondary sulfate minerals is economically and environmentally significant. Compared to what has been determined using bulk sample analysis methods, and bulk XRD most specifically, synchrotron-based XFM analysis shows that a much more diverse set of minerals is present in the precipitates than can be identified by bulk methodologies alone. This allows researchers to clarify what relevant trace-element associations may exist with the varying secondary sulfate minerals. Beyond this, the information necessary to characterize how secondary mineralogy relates to the aqueous geochemistry of drainage waters, allows characterization of any genetic relationships, and provides data that may allow prediction of the likelihood of metal mobilization under mine-waste conditions is also provided.

The coupled μXRF/μXRD mapping of this sample was conducted under essentially identical instrumental conditions as described for the McClean Lake sample. For Lagunas Norte, however, the use of free-standing thin sections that have been removed from a microscopic glass backing has an advantage in that the XRD data collected do not contain a diffuse low-angle scatter from a quartz glass substrate and, thus, the need for that correction is removed, which improves detection of diffraction peaks from the sample between 3.5 and 5 Å. A μXRF compositional map of the intensity of Fe, As, and CuKα fluorescence in a 600 μm × 600 μm area of the sample is shown in Figure 4 (left) (2 μm pixel resolution, 50 ms/pixel acquisition time). Copper is the most abundant element detected everywhere in the map area at concentrations that indicate the predominance of copper-bearing mineral phases in the secondary precipitates. From the μXRF mapping the copper fluorescence intensity varies clearly, but to what degree this reflects differences in the molar proportions of copper in varying copper-bearing minerals or changes in the modal abundance of a single copper mineral phase is unclear. If the distribution of other environmentally relevant trace elements, Fe and As, are examined, they are seen to be distributed heterogeneously at the micrometer scale. For arsenic in particular, a possible correlation in spatial distribution with copper in the sample is evident. Understanding whether this is, in fact, the case and, if so, if this is correlated to varying modal abundance of a single copper-bearing mineral or coupled to varying copper mineralogy, would be very helpful. Again, ideally this requires

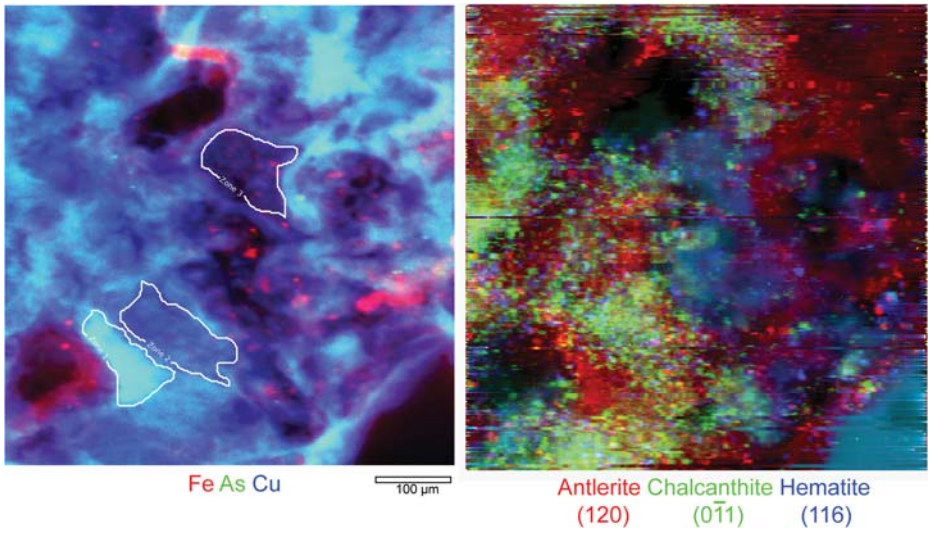

Figure 4. (Left) A three-color, RGB compositional map of the intensity of Fe (red), As (green), and CuKα (blue) fluorescence in a thin section of secondary precipitates collected in waste waters from the Lagunas Norte mine. The image is 600 µm across, each pixel represents acquisition of full XRF energy dispersive spectra every 2 µm at a rate of 50 ms. The white areas labeled 1 through 3 show areas where XRD area detector data shown in Figure 5 were summed for analysis. (Right) Map of the integrated XRD intensity corresponding to the °2θ position of the reflections for antlerite (120) in red, chalcanthite (0$\bar{1}$1) in green, and hematite (116) in blue. In this image, relative intensities of each phase are arbitrary for easier visualization.

a thorough evaluation of how copper mineralogy varies spatially relative to trace-element abundance and speciation.

As was done with the McClean Lake samples, because µXRD data on a per pixel basis are available as part of the map, the variation in chemistry can again be used to define areas where the diffraction data can be summed to evaluate mineralogical variability (Figure 4 left, zones 1, 2, and 3). This summation (Figure 5) reveals that the sample is actually composed of an intimate and complex heterogeneous mixture of two different copper sulfate minerals, chalcanthite ($CuSO_4{}^*5H_2O$) and antlerite ($Cu_3(SO_4)(OH)_4$), something that is virtually impossible to determine using µXRF or µXAFS analysis alone. Application of a reference intensity ratio method (Hubbard and Snyder, 1988) to these summed diffraction patterns allows for a first-order estimate of the relative abundance of each of these two phases in each summed area. This shows rather conclusively that over micrometer-spaced areas of the sample, the ratio of antlerite to chalcanthite varies by more than a factor of 20.

Another advantage in having µXRD data available on a per pixel basis for the maps collected is that once candidate mineral phases have been identified, a map of the intensity of specific mineral reflections that are characteristic can be produced. In this case, for example, the measured X-ray intensities corresponding to the 2θ positions of the

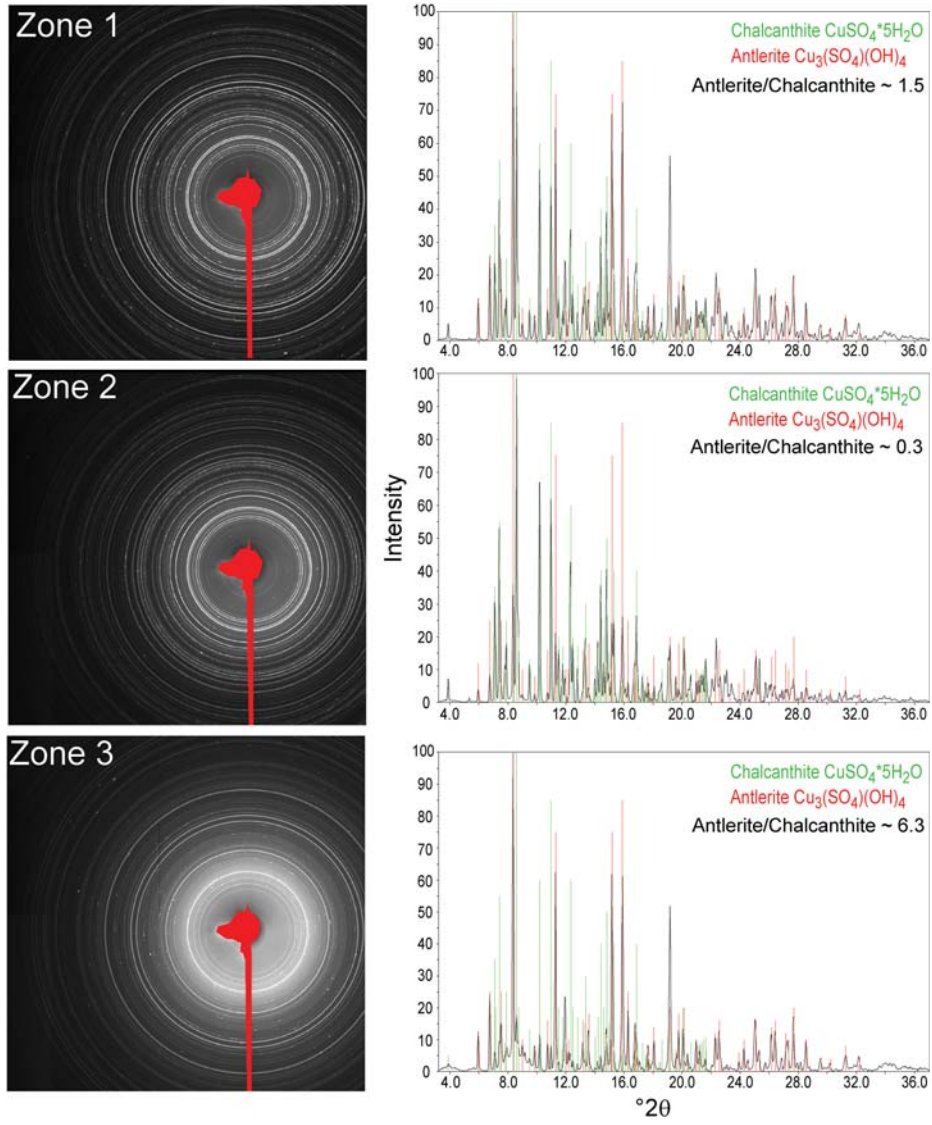

Figure 5. Shown to the left are the summed area detector frames generated for three areas shown in Figure 4 (left) and the integrated °2θ *vs*. intensity patterns on the right. Overlays show XRD standard positions and intensities for chalcanthite and antlerite and the calculated relative abundance ratio of antlerite to chalcanthite based on reference intensity ratios of the diffraction peaks.

antlerite (120), chalcanthite ($0\bar{1}1$), and hematite (116) reflections can be integrated to generate a theoretical map of the mineral distribution of these three phases in the map (Figure 4 right). In cases where such mineral-phase mapping images accurately

report the distribution of each phase uniquely, which for chalcanthite and antlerite in the present sample seems likely, the coupled μXRF data now provide the researcher with the ability to evaluate how trace-element content or molecular speciation is correlated with mineralogy.

Conclusions

The availability of a new generation of high-speed area detectors designed for XRD provides XRF microspectroscopy beamlines with a powerful new tool for megapixel imaging of the spatial heterogeneity in mineralogy within samples with micrometer and sub-micrometer resolutions. In particular, when integrated as a standard detector system at high brightness, *e.g.* undulator-based microprobes such as 13-ID-E, these detectors can generate megapixel streams of XRD area detector data at frame rates of 30 Hz or faster. More importantly, these data streams are coupled synchronously to full energy-dispersive data being provided by new, high-speed count-rate, solid-state XRF detectors and electronics. Such integrated systems give Earth and environmental scientists a unique set of correlated compositional, mineralogical, and spectroscopic data which provide more complete understanding of natural systems.

Acknowledgments

The work described here was performed at GeoSoilEnviroCARS (Sector 13), Advanced Photon Source (APS), Argonne National Laboratory, USA. GeoSoilEnviroCARS is supported by the National Science Foundation – Earth Sciences (EAR-1128799) and Department of Energy – GeoSciences (DE-FG02-94ER14466). This research used resources of the Advanced Photon Source, a U.S. Department of Energy (DOE) Office of Science User Facility operated for the DOE Office of Science by Argonne National Laboratory under Contract No. DE-AC02-06CH11357. Tailings samples from McClean Lake were collected and prepared by John Rowson and AREVA Inc., for which the authors are grateful. Funding for the study of the Lagunas Norte mine was provided by Barrick Gold Corporation and NSERC Create to Dr Heather Jamieson, Queen's University, Kingston, Ontario, Canada.

Guest editor: Thorsten Schäfer

The authors and editors are grateful to anonymous reviewers who offered very helpful input and suggestions. A list of all reviewers is given at the end of the Preface for this volume.

References

Hubbard, C. and Snyder, R. (1988) RIR – measurement and use in quantitative XRD. *Powder Diffraction*, **3**, 74–77.

Jackson, B.P., Williams, P.L., Lanzirotti, A., and Bertsch, P.M. (2005) Evidence for biogenic pyromorphite formation by the nematode Caenorhabditis elegans. *Environmental Science & Technology*, **39**, 5620–56s25.

Lange, K., Rowe, R.K., Jamieson, H., Flemming, R.L., and Lanzirotti, A. (2010) Characterization of geosynthetic clay liner bentonite using micro-analytical methods. *Applied Geochemistry*, **25**, 1056–1069.

Mahoney, J., Slaughter, M., Langmuir, D., and Rowson, J. (2007) Control of As and Ni releases from a uranium mill tailings neutralization circuit: Solution chemistry, mineralogy and geochemical modeling of laboratory study results. *Applied Geochemistry*, **22**, 2758–2776.

Montgomery, A.T. (2012) Metallogenetic controls on Miocene high-sulphidation epithermal gold mineralization, Alto Chicama district, La Libertat, Northern Peru. PhD thesis, Queen's University, Kingston, Ontario, Canada, 436 pp.

Prescher, C. (2014) *Dioptas*, a GUI program for fast analysis of powder X-ray diffraction images. Software package available at https://github.com/Luindil/Dioptas.

Tamura, N., Celestre, R.S., MacDowell, A.A., Padmore, H.A., Spolenak, R., Valek, B.C., Chang, N.M., Manceau, A., and Patel, J.R. (2002) Submicron x-ray diffraction and its applications to problems in materials and environmental science. *Review of Scientific Instruments*, **73**, 1369–1372.

Treiman, A.H., Lanzirotti, A., and Xirouchakis, D. (2004) Ancient water on asteroid 4 Vesta: evidence from a quartz veinlet in the Serra de Magé eucrite meteorite. *Earth and Planetary Science Letters*, **219**, 189–199.

Vogt, S. and Lanzirotti, A. (2013) Trends in X-ray fluorescence microscopy. *Synchrotron Radiation News*, **26**, 32–38.

Walker, S.R., Jamieson, H.E., Lanzirotti, A., Andrade, C.F., and Hall, G.E.M. (2005) The speciation of arsenic in iron oxides in mine wastes from the Giant gold mine, N.W.T.: application of synchrotron micro-XRD and micro-XANES at the grain scale. *The Canadian Mineralogist*, **43**, 1205–1224.